Optical spectroscopy of single colloidal CsPbBr 3 perovskite nanoplatelets

Caixia Huo, Chee Fai Fong, Mohamed-Raouf Amara, Yuqing Huang, Bo Chen, Hua Zhang, Lingjun Guo, Hejun Li, Wei Huang, Carole Diederichs, et al.

Optical spectroscopy of single colloidal $CsPbBr_3$ perovskite nanoplatelets

Caixia Huo,[†,‡,#] Chee Fai Fong,[†,#] Mohamed-Raouf Amara,[†,§,#] Yuqing Huang,[†] Chen Bo,[∥] Hua Zhang,[⊥,ζ] Lingjun Guo,[‡] Hejun Li,[‡] Wei Huang,[&] Carole Diederichs,[,+,§] and Qihua Xiong*[,†,¶]*

[†]Division of Physics and Applied Physics, School of Physical and Mathematical Sciences, Nanyang Technological University, 637371, Singapore

[‡]State Key Laboratory of Solidification Processing, Carbon/Carbon Composites Research Center, Northwestern Polytechnical University, Xi'an 710072, China

[+]MajuLab, International Joint Research Unit UMI 3654, CNRS, Université Côte d'Azur, Sorbonne Université, National University of Singapore, Nanyang Technological University, Singapore

[§]Laboratoire de Physique de l'Ecole Normale Supérieure, ENS, Université PSL, CNRS, Sorbonne Université, Université de Paris, F-75005 Paris, France

[∥]Center for Programmable Materials, School of Materials Science and Engineering, Nanyang Technological University, 50 Nanyang Avenue, Singapore 639798, Singapore

[⊥]Department of Chemistry, City University of Hong Kong, Hong Kong, China

[ζ]Hong Kong Branch of National Precious Metals Material Engineering Research Center (NPMM), City University of Hong Kong, Hong Kong, China.

[&]Shaanxi Institute of Flexible Electronics (SIFE), Northwestern Polytechnical University (NPU), Xi'an, China.

[¶]State Key Laboratory of Low-Dimensional Quantum Physics, Department of Physics, Tsinghua University, Beijing, China.

Keywords: Perovskite, nanoplatelets, photoluminescence, single photon emission, exciton fine structure

Abstract

Optically bright lead halide perovskite nanocrystals of different morphologies ranging from nanocubes to flat nanoplatelets to elongated nanowires have been reported. The morphology of the nanocrystals is expected to affect various properties such as the band edge energy and the electron-hole exchange interaction. However, aside from nanocubes, the investigation of the optical properties of the lead halide perovskite nanocrystals of different morphologies at the single emitter level has been lacking. We have performed optical spectroscopy in single $CsPbBr_3$ nanoplatelets and observed a single photon emission without blinking. Furthermore, the PL emission exhibits excitonic fine structure peaks similar to what has been previously observed in nanocubes. Our work paves the way for further investigations into the excitonic and quantum optics properties when the lateral size and morphology can be further controlled in lead halide perovskite nanocrystals.

Introduction

Lead halide perovskite[1–3] is a class of material which has seen significant resurgence in interest recently in photovoltaic[4], lasing[5], optoelectronics[6,7], polaritonics[8] and quantum optics[9–11]. Lead halide perovskite nanocrystals have been shown to be amenable to shape anisotropy control both in the organo-metal hybrid perovskites[12,13], as well as the all-inorganic perovskite counterparts[14–20]. Partly building on the experience and expertise from past investigations on conventional colloidal nanocrystals[21,22], in the short span of a few years, perovskite nanocrystals with a variety

of morphologies have been reported including nanospheres[17], nanoribbons[19], nanorods[17], nanoplatelets[14–19] and nanowires[20]. Anisotropic shape control is achieved via tuning one or a combination of variables of colloidal synthesis including the temperature[14,16,18], the type of Brønsted acid used[17], the type[15–18,20] as well as the concentration[18,20] of ligands. A different synthesis approach which utilizes the thermodynamic equilibrium of halide and the growth kinetic anisotropy has reportedly produced nanocrystals with highly uniform sizes with shapes ranging from cubes to plates to wires[19]. There is also a report of formation of nanoplatelets via the self-assembly of cubic shape nanocrystals[23].

As demonstrated in other material systems, like size, the shape of a structure can significantly affect the optical[24] and electronic properties[22] giving rise to, for example, polarized[25] and directional PL emission[26] as well as directional charge transport[27]. In lead halide perovskite nanoplatelets and nanowires, the thickness of the structure strongly affects the optical bandgap[14,15,19]. The decrease in the thickness of the nanoplatelets and nanowires is accompanied by the blue shifting of the band edge in the absorption spectrum and the PL emission peak[14,15,19], a manifestation of increasing quantum confinement. This has enabled the production of the much sought after deep blue emitting nanocrystals without resorting to the mixing of halide compositions[14–16]. From temperature around 100K and above, the radiative lifetimes measured in ensemble of nanoplatelets show a linear increase with temperature which is a characteristic of 2D excitons[28]. Also, it has been demonstrated that the emission lifetime of thinner nanowires decreases as expected due to the effects of quantum confinement[20].

Unlike the cubic-shaped perovskite nanocrystals[10,29–33], the investigation of the optical properties of perovskite nanocrystals with anisotropic shapes at the single emitter level has received less attention. In this work, we investigate the optical properties of single $CsPbBr_3$

nanoplatelets produced via a quasi-one-pot colloidal synthesis method. At a temperature of 5K, a single nanoplatelet shows no blinking effect and exhibits highly pure single photon emission with $g^2(0)$=0.1. Furthermore, the PL emission from the nanoplatelets exhibits excitonic fine structure splitting. Our work highlights the importance of investigating the effects of the morphology of halide-based perovskite nanocrystals at the single emitter level as this will allow us another degree of freedom to tailor the electronic or optical properties to their prospective applications.

Results and discussion

To synthesize the $CsPbBr_3$ nanoplatelets, a mixture of tetraoctylammonium bromide and toluene was injected into a flask containing a mixture of lead acetate, oleylamine, oleic acid, dodecyl benzene sulfonic acid, octadecene and cesium carbonate at 130°C followed by cooling of the flask in a water bath (see Materials and Methods section for further details, and supplementary information Figure S1). The morphology of the resulting nanoplatelets was confirmed via transmission electron microscopy (TEM) and atomic force microscopy (AFM) measurements. At high concentrations, the nanoplatelets tend to stack face-to-face[14,15] and lie on their edge when deposited onto the TEM grid (Figure 1a). Whereas at low concentration, single nanoplatelets can be spatially isolated and tend to lie flat on a substrate (Figure 1b). Since the nanoplatelet stacks are lying on their edge in the TEM images, this allows us to measure the thickness of individual nanoplatelets to be 2.6±0.4 nm with a mean lateral size of 23.5±3.2 nm (refer to supplementary information Figure S2 for the histograms). From AFM measurements (Figure 1c), the thickness of the nanoplatelets is determined to be between 2 - 5 nm which is consistent with that obtained from TEM images.

The low temperature ensemble PL spectrum shows multiple sharp peaks with an average full width at half maximum of 11 meV (Figure 1d). These peaks can be attributed to the presence of nanoplatelets with different thicknesses[14,15,19]. By comparing our data with that reported in the literature[14,15], the emission peaks originating from nanoplatelets of 3 monolayers (ML) to 7 ML are identified and labelled in Figure 1d. A nanoplatelet of *n* monolayers consists of *n* number of $PbBr_6^{4-}$ octahedral units across the thickness of the nanoplatelet[15,19]. Nanoplatelet thicknesses of more than 7 ML cannot be clearly determined as the spacing between peaks becomes smaller with increasing thickness. The identified number of monolayers is consistent with the range of the thickness (2 – 5 nm) measured with AFM. The peak at 2.32 eV most likely arises from stacked nanoplatelets which essentially behave like a bulk emitter[34]. Thinner nanoplatelets tend to have their band edge and PL emission at higher energies and vice versa (see supplementary information Figure S3 for further analysis). At room temperature, the absorption and PL measurements on ensemble nanoplatelets also show broad spectra with multiple peaks (Figure 1d inset).

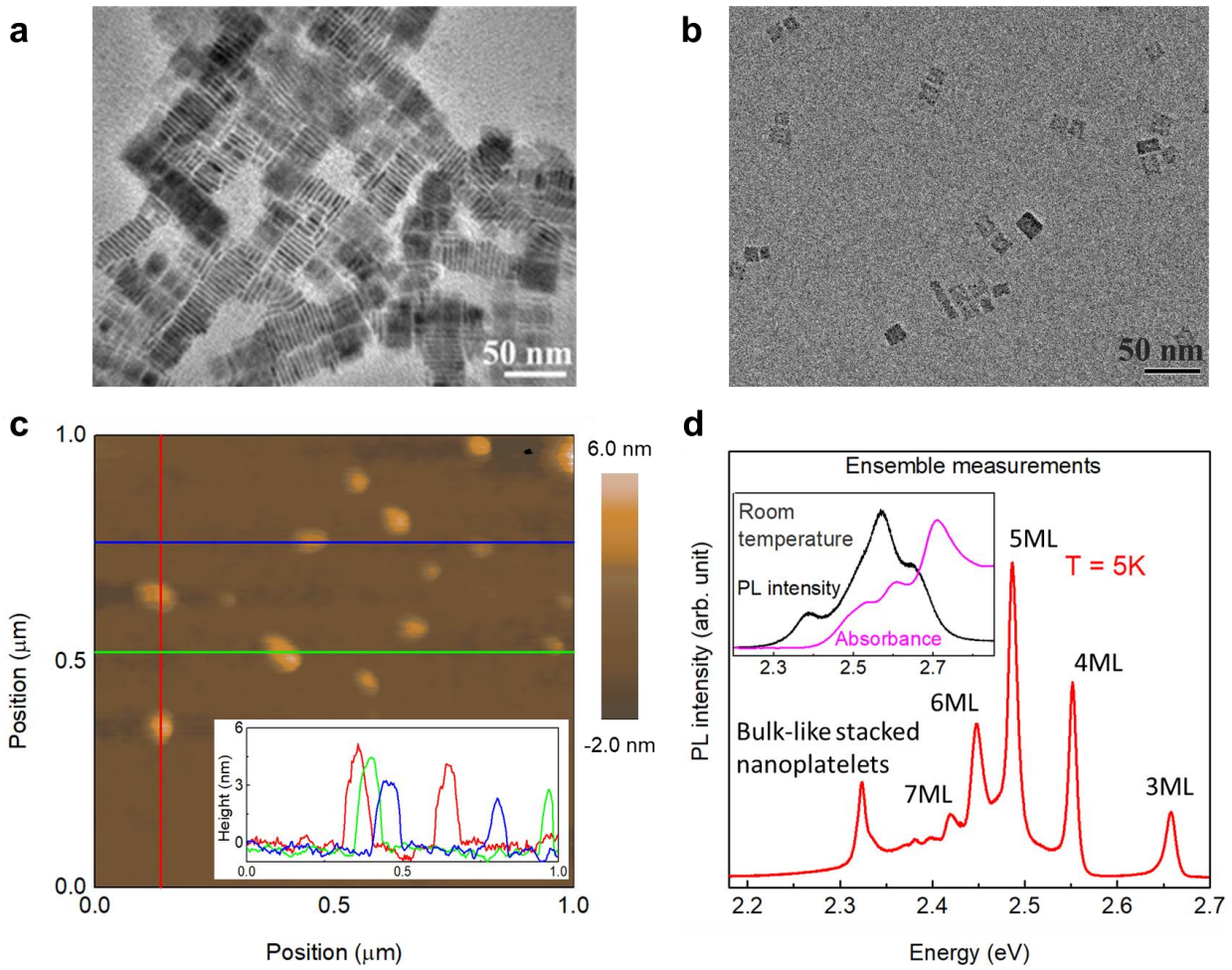

Figure. 1. TEM images of the $CsPbBr_3$ nanoplatelets prepared from solutions with high (a) and low concentration (b) of nanoplatelets. The scale bars indicate 50 nm in both (a) and (b). In (a), a mixture of nanoplatelets lying flat and edge-on can be seen. Spatially isolated nanoplatelets lying flat can be seen in (b) enabling single emitter optical characterization. (c) AFM topography image of individual and aggregated $CsPbBr_3$ nanoplatelets. (Inset) Color-coded height profiles corresponding to the line cuts indicate that the thickness of the nanoplatelets is about 2 – 5 nm. (d) Low temperature nanoplatelets ensemble PL spectrum showing multiple sharp peaks with an average full width at half maximum of 11 meV. The multiple peaks indicate the presence of nanoplatelets with varying thicknesses in the ensemble. The corresponding nanoplatelet

thicknesses of the emission peaks are labelled in units of monolayers (ML). (Inset) Absorption and PL emission spectra of nanoplatelets ensemble measured at room temperature.

In order to obtain a better understanding of the optical properties of single $CsPbBr_3$ nanoplatelets, low-temperature (T = 5 K) optical spectroscopy experiments were conducted. Figure 2a shows the PL spectra of a nanoplatelets under increasing excitation power. The PL emission arises from an exciton given that its intensity increases linearly with excitation power (Fig. 2b). For a different nanoplatelet, an additional peak appears at about 17 meV away on the lower energy side of the exciton peak under high excitation power (Figure S4 in supplementary information). This additional peak could correspond to emission from a trion.

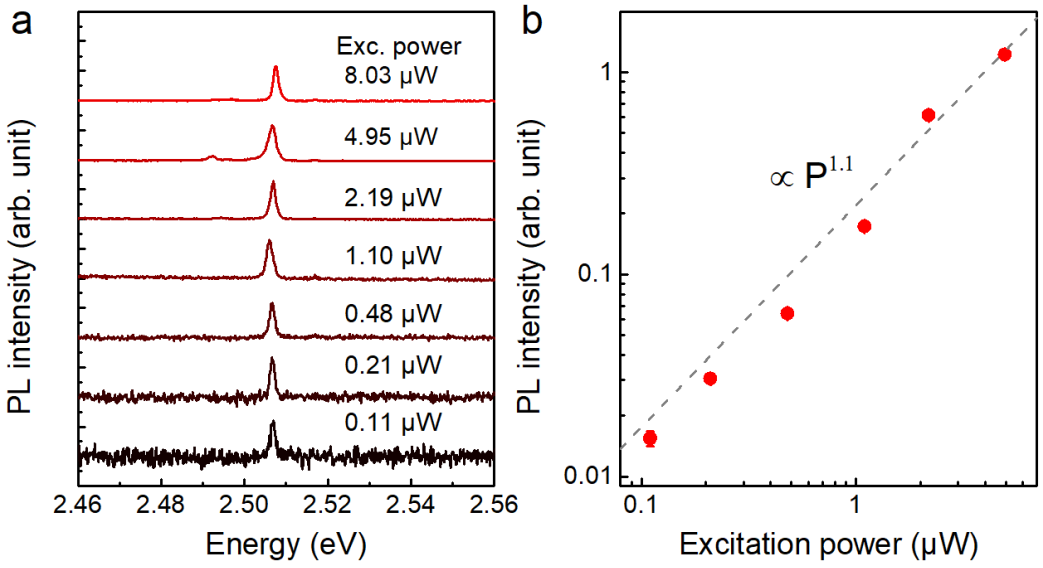

Figure. 2 (a) PL spectra of a nanoplatelets under increasing excitation power. (b) Plotted on a log-log scale the integrated PL intensity increases linearly to the excitation power raised to the exponent of ~1.

Figure 3a shows the PL emission spectrum from a different single nanoplatelet, with a full width at half maximum (FWHM) of 0.94 meV. The time-resolved PL decay measurement (Figure 3b) is fitted with a single exponential decay function convolved with the instrument response function (IRF), giving a PL decay time of 79 ± 8 ps. The decay times reported in the literature for nanocubes are on the order of 200 ps[10,32]. The relatively short decay time measured in the nanoplatelets here could be due to the presence of giant oscillator strength transition[22]. Figure 3c shows the PL intensity time trace with a time bin of 10 ms of the same nanoplatelet emission – under pulsed excitation and recorded with avalanche photodiodes – indicating no blinking behavior at this timescale. This is corroborated by the PL intensity distribution (Figure 3d) indicating only emission from an "on" state, which is largely consistent with a Poisson distribution fit. We further investigated the nature of the emission of the single nanoplatelet, and more specifically the photon emission statistics, by measuring with a Hanbury-Brown and Twiss setup the second-order intensity correlation function $g^2(\tau) = \langle I(\tau)I(t+\tau)\rangle / \langle I(t)\rangle^2$, where τ is the time delay between the detectors and $I(t)$ is the PL intensity at time t. The excitation power used in the measurements here were kept low such that only one exciton was created within the nanoplatelet per excitation pulse. Under pulsed excitation, the coincidence counts histogram (Figure 3e) shows a clear antibunching effect as indicated by the inhibited coincidence counts at the time delay of $\tau = 0$, which is the signature of a sub-Poissonian emission. In particular, at zero time delay, the second-order intensity correlation is measured to be $g^2(\tau=0) = 0.1 < 0.5$, signifying the single photon nature of the PL emission from a single nanoplatelet. Figure 3f is the plot of the $g^2(\tau)$ on a logarithmic time scale. The $g^2(\tau)$ is normalized to the mean of the data within the plot. The $g^2(\tau)$ tends to 1 at long time scales as indicated by the dashed line indicating the blinking is strongly suppressed in the PL emission. Two other examples of $g^2(\tau)$ are presented in the supplementary information Figure S5.

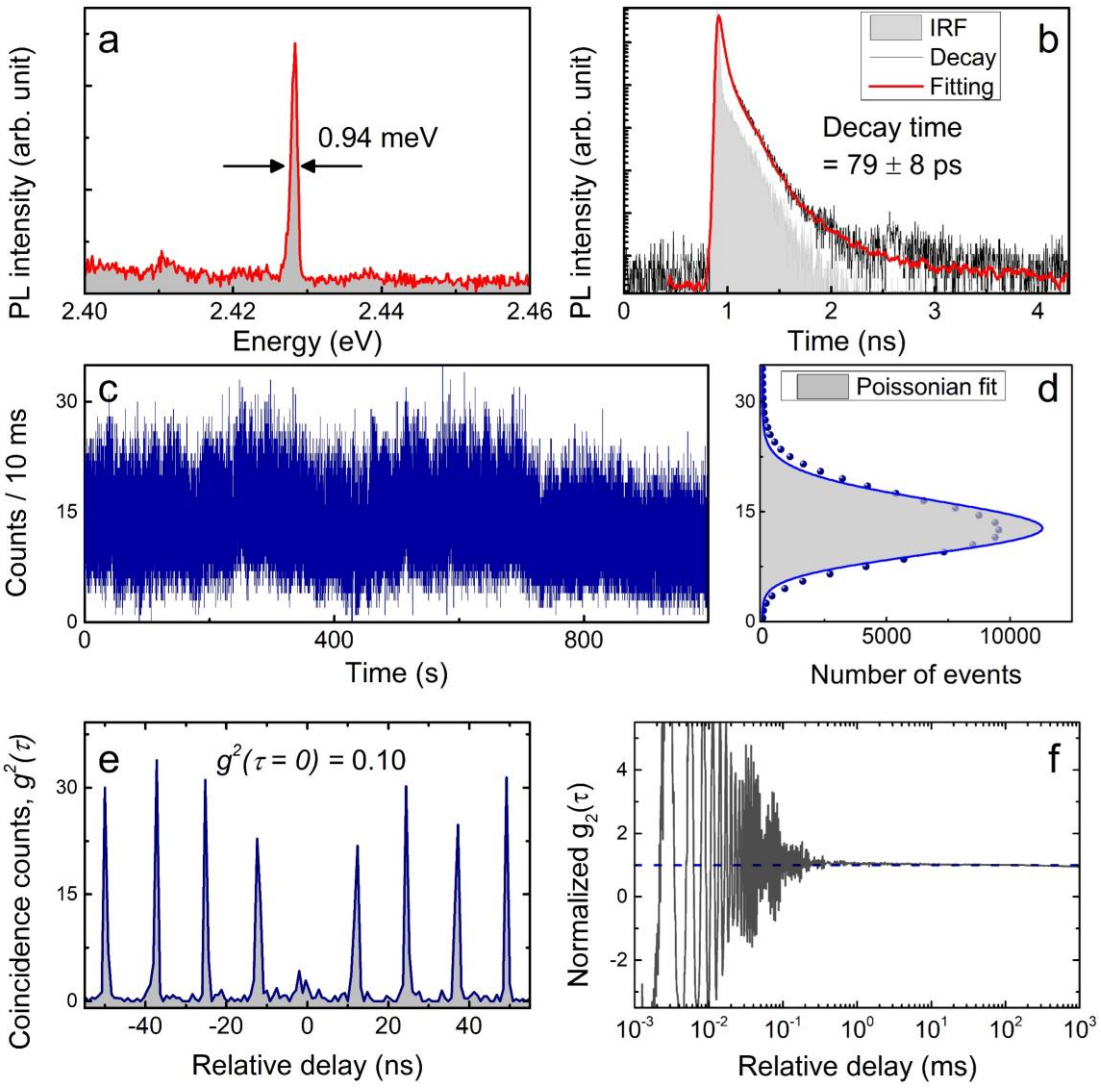

Figure 3 (a) PL emission spectrum of an individual $CsPbBr_3$ nanoplatelet that exhibits a single peak with a FWHM of 0.94 meV at 5.0 Kelvin. (b), PL decay (black) and fitted curve (red) of this single $CsPbBr_3$ nanoplatelet. The instrument response function (IRF) (shaded gray) – measured at 2.431 eV (510 nm) – is taken into consideration in the fitting of the PL decay. (c) PL intensity time trace plotted with a binning time of 10 ms. (d) Distribution of the PL intensity in (c) showing only an emission from an "on" state. The distribution of the PL intensity is largely consistent with the Poissonian fit. (e) Second-order PL intensity correlation $g^2(\tau)$ measured for a single $CsPbBr_3$ nanoplatelet under pulsed excitation showing a clear antibunching at zero time delay. (f) Plot of

the normalized second-order intensity correlation function on a logarithmic time scale. Dash line corresponds to normalized $g^2(\tau) = 1$ indicating the absence of blinking in the PL emission.

For this work, measurements were focused on emission peaks with energies above 2.4 eV to avoid the bulk-like stacked nanoplatelets and multiple single nanoplatelets were studied. The antibunching signature in the second-order intensity correlation was also observed in other single nanoplatelets (see supplementary information). In addition, the PL emission of the single nanoplatelets exhibits a different number of peaks. Figures 4a-c present the exemplary spectra of PL emission from single nanoplatelets showing one, two and three peaks respectively. The splittings ΔE, ΔE_1 and ΔE_2, as labelled in Figures 4b and 4c are deduced from the fittings to be 0.71 ± 0.06 meV, 0.57 ± 0.02 meV and 1.84 ± 0.13 meV respectively. Figures 4d-f are the polar plots of the polarization dependence of the intensity of each peak present in the corresponding spectra in Figures 4a-c. A degree of polarization of almost 80% is measured in the nanoplatelet in Figure 4a. The high degree of polarization could be facilitated by the dielectric antenna effect induced by the elongation of the lateral plane[35]. In the cases of nanoplatelets exhibiting multiple emission peaks (Figure 4b, c), the polarizations of the two lower energy peaks are almost orthogonal to each other, whereas the higher energy peak is almost co-polarized as the lower energy peak. The observed polarization dependence of the emission peaks strongly indicates that they arise from exciton fine structure.

In the PL spectra, the lowest energy peak tends to be the most intense since the emission from the lowest lying energy level tends to be the most heavily populated energy level as expected from thermal distribution. The higher energy peaks should not originate from excited states which are expected to be ~200 meV away[36]. The additional peak could not be from biexcitons which should

be ~100 meV on the lower energy side of the exciton[37]. Besides, biexciton emission could not explain the spectra with 3 peaks. Furthermore, the polarization dependence of the PL emission is consistent with previous reports[32,33,38] which claimed that the multiple peaks observed arose from the excitonic fine structure levels of single nanocrystals. Given the polarization dependence, these peaks are unlikely to arise from surface or trap states. Therefore, we conclude that the multiple peaks in the PL spectra arise from the exciton fine structure.

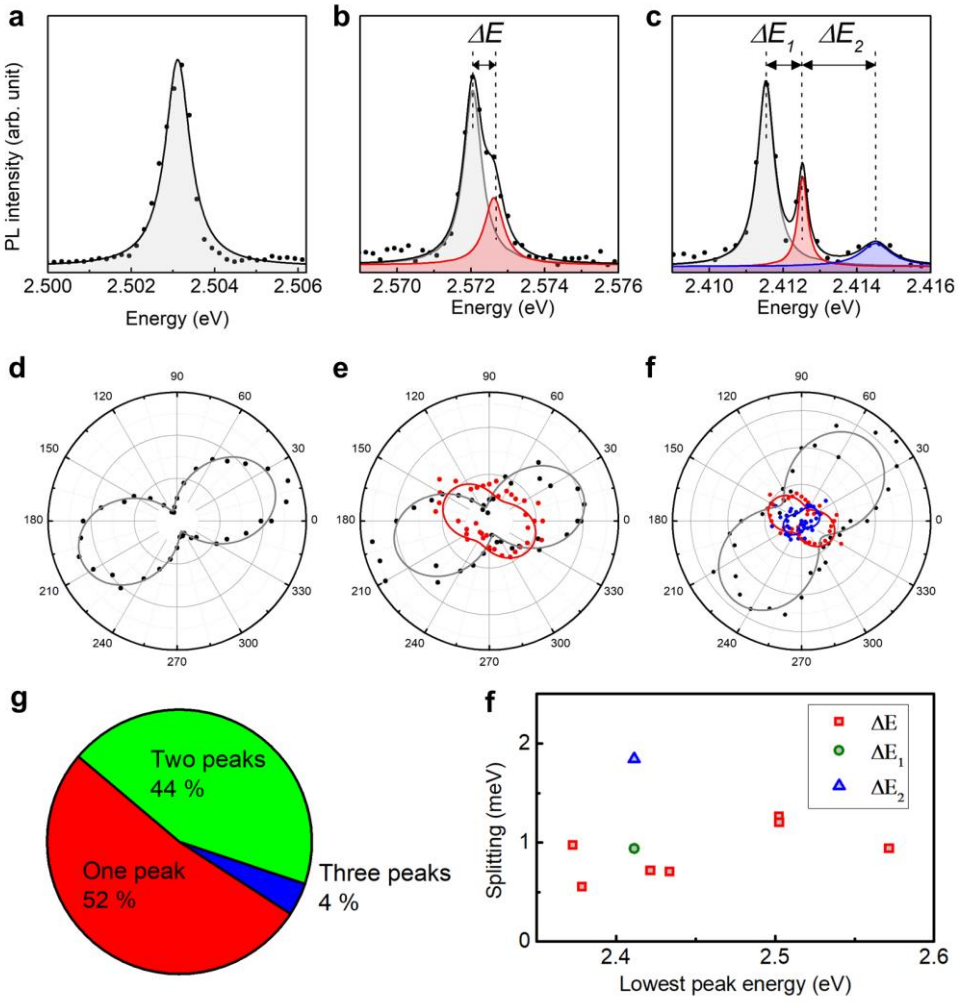

Figure. 4 Excitonic fine structure of the $CsPbBr_3$ nanoplatelets. PL spectra of the single nanoplatelets with one peak (a), two peaks (b) and three peaks (c) as well as the corresponding linear polarization properties (d-f). In (b) and (c), the splittings are labeled ΔE, ΔE_1 and ΔE_2 and

are deduced from the fittings to be 0.71 meV, 0.57 meV and 1.84 meV respectively. (g) The relative abundance of the single $CsPbBr_3$ nanoplatelet with one, two and three emission peaks. (h) Summary of the fine structure splitting of $CsPbBr_3$ nanoplatelets with two and three emission peaks.

In lead halide perovskite nanocrystals, the PL emission arises from excitons in the triplet state. The triplet state could split into non-degenerate states depending on the crystal phase and the shape of the nanocrystal[39]. For an isotropically shaped nanocrystal in the cubic crystal phase, the triplet states are expected to be degenerate and thus no splitting should be observed. In the tetragonal phase – which has a lower symmetry than the cubic phase –the triplet state will split into a doublet whereas in the orthorhombic phase, the triplet state will split into three nondegenerate states[33,39]. For a completely anisotropically shaped nanocrystals – in which all three dimensions are of unequal length, the triplet states are split into three nondegenerate states regardless of the crystal phase[39]. The reduction of the symmetry of the crystal phase by Rashba effects could also be responsible for splitting the triplet state into three nondegenerate states[32].

At low temperature of 5 K, the nanoplatelets are expected to be in the orthorhombic phase. However, the nanoplatelets in both orthorhombic and tetragonal phases could coexist within the same batch of colloidal synthesis[33] or even the same nanocrystal[40] as it has been previously shown for cubic shape nanocrystals. Given the anisotropic shape of the nanoplatelets, the triplet states should be completely split. Nonetheless, emission with one or two peaks were still observed in the nanoplatelets. This could be due to the low population of the highest energy level or the insufficient resolution of the detector to distinguish the multiple peaks in case of splittings smaller than 250 μeV . Furthermore, the observation of the multiple peaks in the PL emission also depends on the

orientation of the nanocrystal[32]. The combination of these factors could explain the observation of nanoplatelets with one, two and three peaks in the PL emission.

As described in a previous paragraph, the triplet state is expected to split into three nondegenerate states due to the anisotropic shape of the NPLs. However, most of the measured single NPLs exhibits one or two peaks in the PL spectra (Figure 4g). The relative lack of NPLs with three peaks in the emission could be due to the low population of the highest energy level. This could also suggest that the splitting of the degenerate energy levels is not as strongly governed by the shape anisotropy.

The fine structure splittings (Figure 4f) observed in the nanoplatelets are comparable to previously reported values for that in nanocubes[31–33,38,41,42] despite predictions that the splitting should increase with shape anisotropy[39]. Nonetheless, the predicted effect was for nanocubes with a relatively small shape anisotropy and thus may not apply directly to nanoplatelets which are more highly anisotropic. A possible reason for the comparable splittings observed in nanoplatelets and nanocubes could be that the excitons are only in the weak or intermediate confinement regime due to the large lateral dimensions of the nanoplatelets.

Conclusions

We have performed optical spectroscopy on single $CsPbBr_3$ nanoplatelets produced via a quasi-one-pot synthesis method. The emission from the single nanoplatelet showed no blinking and is single photon in nature with a measured $g^2(0) = 0.10$ at a temperature of 5 K. In addition, excitonic fine structures were observed in the PL spectra. Despite their highly anisotropic morphology the observed fine structure splitting values are comparable to that reported for nanocubes. Our work

highlights the importance of investigating the effects of the morphology of halide-based perovskites, which could be utilized as a degree of freedom to manipulate on their electronic and optical properties.

Materials and methods

Chemicals: Cesium carbonate (Cs_2CO_3, 99.9%), lead acetate trihydrate ($Pb(OAc)_2 \cdot 3H_2O$, 99.99%), oleylamine (OLA, 70%), oleic acid (OA, 93%), 1,4-dodecyl benzene sulfonic acid (1,4-DBSA, 95%), tetraoctylammonium bromide (TOAB, 99%), 1-octadecene (ODE, 90%), toluene (99.8%) and hexane (anhydrous, 99%) are used for the synthesis of $CsPbBr_3$ nanoplatelets.

Synthesis: Cs_2CO_3 (0.0889 g, 0.273 mmol), $Pb(OAc)_2 \cdot 3H_2O$ (0.309 g, 0.945 mmol), 1,4-DBSA (1.8067 g, 5.534 mmol), OA (1.5 ml), OLA (1.5 ml) and ODE (15 ml) are added into a 100 ml 3-neck flask. The flask is evacuated and refilled with N_2 three times to ensure an inert atmosphere. Then the flask is heated under vacuum for 1 h at 130 ℃. After the mixture of chemicals have dissolved completely, the pump is turned off and the flask is refilled with N_2. The temperature of the flask is kept at 130 ℃ for 30 min under N_2 atmosphere. TOAB (1.122 g, 2.055 mmol) is added into the toluene (3 ml) and heated at 130 ℃ till the TOAB dissolves completely. The TOAB-toluene solution is then quickly injected into the flask while keeping the flask at 130 ℃ for 5 seconds. Then the flask is cooled down in a water bath.

Purification of the $CsPbBr_3$ nanoplatelets: The crude solution is centrifuged for 5 min at 5000 rpm and the supernatant is discarded. The precipitate is dispersed in hexane and centrifuged again for 5 min at 5000 rpm. The dispersion of the precipitate and centrifugation step are repeated twice. The supernatant is then separated from the precipitate and kept for investigations.

Sample preparation: The colloidal dispersion is diluted in 5-wt% poly(methyl methacrylate) (PMMA) in toluene and spin-coated on distributed Bragg reflectors (5000 rpm/min) for single nanoplatelet spectroscopy.

Optical characterization: The absorption spectrum of the nanoplatelet ensemble was measured using a PerkinElmer Lambda 950 UV-vis-IR spectrometer. The nanoplatelet sample dispersed in hexane is held in a cuvette for the measurement.

For single nanoplatelets, the optical measurements are performed with a home-built confocal micro-photoluminescence setup. The samples are put in a cryostat fixed on a xyz translation stage. All measurements are carried out at a low temperature of 5 K. A Ti:sapphire femtosecond-pulsed laser with ~100 fs pulses at 80 MHz is used as the excitation source. The emission of the laser is frequency-doubled to output 457 nm pulses and is focused (50× objective lens, NA = 0.65) onto the sample. The laser spot size at focus is about 1 μm in width. The excitation fluence is typically around 1 W/cm^2.

The PL emission, which is separated from the excitation laser by a combination of a 90:10 beamsplitter and a longpass filter, is dispersed in a 320 mm spectrometer together with a 1800 lines/mm grating. For the time-averaged measurements, the PL emission is detected using a liquid nitrogen cooled Si CCD detector. For time-resolved decay measurements, the PL emission is first spectrally filtered with the spectrometer and the filtered PL emission is detected with an avalanche photon detector (APD) connected to a single photon counting module (PicoHarp 300). A Hanbury-Brown and Twiss setup is used to characterize the single photon nature of the PL emission. In this case, the spectrally filtered PL emission is directed to a 50/50 beam splitter and two corresponding APDs located at each output of the 50/50 beamsplitter. The overall temporal resolution of the time-resolved setup for the range of wavelengths under investigation is measured to be about 40 ps.

For polarization resolved measurements, a motorized half-wave plate and a linear polarizer is placed before the entrance slit of the spectrometer. The half-wave plate is rotated while the linear polarizer is fixed to ensure that any change in the PL intensity is due to the intrinsic polarization of the emission and not due to the polarization response of the spectrometer grating.

ASSOCIATED CONTENT

The schematic of the synthesis, the statistics of the dimensions of the nanoplatelets and a summary of the reported fine structure splittings are included in the supplementary info document.

AUTHOR INFORMATION

Corresponding Author

*Email: qihua@ntu.edu.sg

*Email: carole.diederichs@phys.ens.fr

Author Contributions

C.H. and M.-R.A. synthesized the perovskite nanoplatelets and prepared the samples. C.H., C.F.F., M.-R.A. and Y.H. performed the experimental measurements and analyzed the results. C.H. performed the TEM characterizations with C.B. under the supervision of H.Z. C.H. and C.F.F. wrote the manuscript with input from all co-authors. C.D. and Q.X. supervised the project.

[#]C.H., C.F.F. and M.-R.A. contributed equally to this work.

Funding Sources

Q.X. gratefully acknowledges the financial support from Singapore National Research Foundation via and Ministry of Education via AcRF Tier3 Programme (MOE2018-T3-1-002) and Tier2 grants (MOE2017-T2-1-040 and MOE2018-T2-2-068). C.D. acknowledges the financial support from the French National Research Agency (ANR IPER-Nano2, Grant No. ANR-18-CE30-0023-01). Both Q.X. and C.D. acknowledge the Merlion programme (M40822392), a joint French-Singaporean collaboration. H.Z. thanks the financial support from ITC via Hong Kong Branch of National Precious Metals Material Engineering Research Center, and the start-up grant (Project No. 9380100) and grants (Project No. 9610478 and 1886921) in City University of Hong Kong. C.H. acknowledges financial support from the China Scholarship Program, 2018 (CSC No. 201806290061). Y.H. acknowledges financial support from the Knut and Alice Wallenberg Foundation.

REFERENCES

(1) Møller, C. K. A Phase Transition in Cæsium Plumbochloride. *Nature* **1957**, *180* (4593), 981–982. https://doi.org/10.1038/180981a0.

(2) Ha, S. T.; Liu, X.; Zhang, Q.; Giovanni, D.; Sum, T. C.; Xiong, Q. Synthesis of Organic-Inorganic Lead Halide Perovskite Nanoplatelets: Towards High-Performance Perovskite Solar Cells and Optoelectronic Devices. *Advanced Optical Materials* **2014**, *2* (9), 838–844. https://doi.org/10.1002/adom.201400106.

(3) Protesescu, L.; Yakunin, S.; Bodnarchuk, M. I.; Krieg, F.; Caputo, R.; Hendon, C. H.; Yang, R. X.; Walsh, A.; Kovalenko, M. V. Nanocrystals of Cesium Lead Halide Perovskites ($CsPbX_3$, X = Cl, Br, and I): Novel Optoelectronic Materials Showing Bright Emission with Wide Color Gamut. *Nano Letters* **2015**, *15* (6), 3692–3696. https://doi.org/10.1021/nl5048779.

(4) A Decade of Perovskite Photovoltaics. *Nat Energy* **2019**, *4* (1), 1–1. https://doi.org/10.1038/s41560-018-0323-9.

(5) Zhang, Q.; Ha, S. T.; Liu, X.; Sum, T. C.; Xiong, Q. Room-Temperature Near-Infrared High-Q Perovskite Whispering-Gallery Planar Nanolasers. *Nano Letters* **2014**, *14* (10), 5995–6001. https://doi.org/10.1021/nl503057g.

(6) Cao, Y.; Wang, N.; Tian, H.; Guo, J.; Wei, Y.; Chen, H.; Miao, Y.; Zou, W.; Pan, K.; He, Y.; et al. Perovskite Light-Emitting Diodes Based on Spontaneously Formed Submicrometre-Scale Structures. *Nature* **2018**, *562* (7726), 249–253. https://doi.org/10.1038/s41586-018-0576-2.

(7) Fong, C. F.; Yin, Y.; Chen, Y.; Rosser, D.; Xing, J.; Majumdar, A.; Xiong, Q. Silicon Nitride Nanobeam Enhanced Emission from All-Inorganic Perovskite Nanocrystals. *Opt. Express* **2019**, *27* (13), 18673. https://doi.org/10.1364/OE.27.018673.

(8) Su, R.; Diederichs, C.; Wang, J.; Liew, T. C. H.; Zhao, J.; Liu, S.; Xu, W.; Chen, Z.; Xiong, Q. Room-Temperature Polariton Lasing in All-Inorganic Perovskite Nanoplatelets. *Nano Letters* **2017**, *17* (6), 3982–3988. https://doi.org/10.1021/acs.nanolett.7b01956.

(9) Becker, M. A.; Scarpelli, L.; Nedelcu, G.; Rainò, G.; Masia, F.; Borri, P.; Stöferle, T.; Kovalenko, M. V.; Langbein, W.; Mahrt, R. F. Long Exciton Dephasing Time and Coherent Phonon Coupling in $CsPbBr_2Cl$ Perovskite Nanocrystals. *Nano Lett.* **2018**, *18* (12), 7546–7551. https://doi.org/10.1021/acs.nanolett.8b03027.

(10) Utzat, H.; Sun, W.; Kaplan, A. E. K.; Krieg, F.; Ginterseder, M.; Spokoyny, B.; Klein, N. D.; Shulenberger, K. E.; Perkinson, C. F.; Kovalenko, M. V.; et al. Coherent Single-Photon Emission from Colloidal Lead Halide Perovskite Quantum Dots. *Science* **2019**, *363* (6431), 1068–1072. https://doi.org/10.1126/science.aau7392.

(11) Rainò, G.; Becker, M. A.; Bodnarchuk, M. I.; Mahrt, R. F.; Kovalenko, M. V.; Stöferle, T. Superfluorescence from Lead Halide Perovskite Quantum Dot Superlattices. *Nature* **2018**, *563* (7733), 671–675. https://doi.org/10.1038/s41586-018-0683-0.

(12) Schmidt, L. C.; Pertegás, A.; González-Carrero, S.; Malinkiewicz, O.; Agouram, S.; Mínguez Espallargas, G.; Bolink, H. J.; Galian, R. E.; Pérez-Prieto, J. Nontemplate Synthesis of CH3NH3PbBr3 Perovskite Nanoparticles. *J. Am. Chem. Soc.* **2014**, *136* (3), 850–853. https://doi.org/10.1021/ja4109209.

(13) Tyagi, P.; Arveson, S. M.; Tisdale, W. A. Colloidal Organohalide Perovskite Nanoplatelets Exhibiting Quantum Confinement. *J. Phys. Chem. Lett.* **2015**, *6* (10), 1911–1916. https://doi.org/10.1021/acs.jpclett.5b00664.

(14) Bekenstein, Y.; Koscher, B. A.; Eaton, S. W.; Yang, P.; Alivisatos, A. P. Highly Luminescent Colloidal Nanoplates of Perovskite Cesium Lead Halide and Their Oriented Assemblies. *J. Am. Chem. Soc.* **2015**, *137* (51), 16008–16011. https://doi.org/10.1021/jacs.5b11199.

(15) Akkerman, Q. A.; Motti, S. G.; Srimath Kandada, A. R.; Mosconi, E.; D'Innocenzo, V.; Bertoni, G.; Marras, S.; Kamino, B. A.; Miranda, L.; De Angelis, F.; et al. Solution Synthesis Approach to Colloidal Cesium Lead Halide Perovskite Nanoplatelets with Monolayer-Level Thickness Control. *J. Am. Chem. Soc.* **2016**, *138* (3), 1010–1016. https://doi.org/10.1021/jacs.5b12124.

(16) Pan, A.; He, B.; Fan, X.; Liu, Z.; Urban, J. J.; Alivisatos, A. P.; He, L.; Liu, Y. Insight into the Ligand-Mediated Synthesis of Colloidal $CsPbBr_3$ Perovskite Nanocrystals: The Role of Organic Acid, Base, and Cesium Precursors. *ACS Nano* **2016**, *10* (8), 7943–7954. https://doi.org/10.1021/acsnano.6b03863.

(17) Sun, S.; Yuan, D.; Xu, Y.; Wang, A.; Deng, Z. Ligand-Mediated Synthesis of Shape-Controlled Cesium Lead Halide Perovskite Nanocrystals *via* Reprecipitation Process at Room Temperature. *ACS Nano* **2016**, *10* (3), 3648–3657. https://doi.org/10.1021/acsnano.5b08193.

(18) Almeida, G.; Goldoni, L.; Akkerman, Q.; Dang, Z.; Khan, A. H.; Marras, S.; Moreels, I.; Manna, L. Role of Acid–Base Equilibria in the Size, Shape, and Phase Control of Cesium Lead Bromide Nanocrystals. *ACS Nano* **2018**, *12* (2), 1704–1711. https://doi.org/10.1021/acsnano.7b08357.

(19) Dong, Y.; Qiao, T.; Kim, D.; Rossi, D.; Ahn, S. J.; Son, D. H. Controlling Anisotropy of Quantum-Confined $CsPbBr_3$ Nanocrystals by Combined Use of Equilibrium and Kinetic Anisotropy. *Chem. Mater.* **2019**, *31* (15), 5655–5662. https://doi.org/10.1021/acs.chemmater.9b01515.

(20) Imran, M.; Di Stasio, F.; Dang, Z.; Canale, C.; Khan, A. H.; Shamsi, J.; Brescia, R.; Prato, M.; Manna, L. Colloidal Synthesis of Strongly Fluorescent $CsPbBr_3$ Nanowires with Width Tunable down to the Quantum Confinement Regime. *Chem. Mater.* **2016**, *28* (18), 6450–6454. https://doi.org/10.1021/acs.chemmater.6b03081.

(21) Schliehe, C.; Juarez, B. H.; Pelletier, M.; Jander, S.; Greshnykh, D.; Nagel, M.; Meyer, A.; Foerster, S.; Kornowski, A.; Klinke, C.; et al. Ultrathin PbS Sheets by Two-Dimensional Oriented Attachment. *Science* **2010**, *329* (5991), 550–553. https://doi.org/10.1126/science.1188035.

(22) Ithurria, S.; Tessier, M. D.; Mahler, B.; Lobo, R. P. S. M.; Dubertret, B.; Efros, Al. L. Colloidal Nanoplatelets with Two-Dimensional Electronic Structure. *Nature Mater* **2011**, *10* (12), 936–941. https://doi.org/10.1038/nmat3145.

(23) Gomez, L.; Lin, J.; de Weerd, C.; Poirier, L.; Boehme, S. C.; von Hauff, E.; Fujiwara, Y.; Suenaga, K.; Gregorkiewicz, T. Extraordinary Interfacial Stitching between Single All-Inorganic Perovskite Nanocrystals. *ACS Appl. Mater. Interfaces* **2018**, *10* (6), 5984–5991. https://doi.org/10.1021/acsami.7b17432.

(24) Kan, S.; Mokari, T.; Rothenberg, E.; Banin, U. Synthesis and Size-Dependent Properties of Zinc-Blende Semiconductor Quantum Rods. *Nature Mater* **2003**, *2* (3), 155–158. https://doi.org/10.1038/nmat830.

(25) Hu, J.; Li, L.; Yang, W.; Manna, L.; Wang, L.; Alivisatos, A. P. Linearly Polarized Emission from Colloidal Semiconductor Quantum Rods. *Science* **2001**, *292* (5524), 2060–2063. https://doi.org/10.1126/science.1060810.

(26) Scott, R.; Heckmann, J.; Prudnikau, A. V.; Antanovich, A.; Mikhailov, A.; Owschimikow, N.; Artemyev, M.; Climente, J. I.; Woggon, U.; Grosse, N. B.; et al. Directed Emission of CdSe Nanoplatelets Originating from Strongly Anisotropic 2D Electronic Structure. *Nature Nanotech* **2017**, *12* (12), 1155–1160. https://doi.org/10.1038/nnano.2017.177.

(27) Huynh, W. U.; Dittmer, J. J.; Alivisatos, A. P. Hybrid Nanorod-Polymer Solar Cells. *Science* **2002**, *295* (5564), 2425–2427. https://doi.org/10.1126/science.1069156.

(28) Li, J.; Luo, L.; Huang, H.; Ma, C.; Ye, Z.; Zeng, J.; He, H. 2D Behaviors of Excitons in Cesium Lead Halide Perovskite Nanoplatelets. *J. Phys. Chem. Lett.* **2017**, *8* (6), 1161–1168. https://doi.org/10.1021/acs.jpclett.7b00017.

(29) Park, Y.-S.; Guo, S.; Makarov, N. S.; Klimov, V. I. Room Temperature Single-Photon Emission from Individual Perovskite Quantum Dots. *ACS Nano* **2015**, *9* (10), 10386–10393. https://doi.org/10.1021/acsnano.5b04584.

(30) Hu, F.; Zhang, H.; Sun, C.; Yin, C.; Lv, B.; Zhang, C.; Yu, W. W.; Wang, X.; Zhang, Y.; Xiao, M. Superior Optical Properties of Perovskite Nanocrystals as Single Photon Emitters. *ACS Nano* **2015**, *9* (12), 12410–12416. https://doi.org/10.1021/acsnano.5b05769.

(31) Yin, C.; Chen, L.; Song, N.; Lv, Y.; Hu, F.; Sun, C.; Yu, W. W.; Zhang, C.; Wang, X.; Zhang, Y.; et al. Bright-Exciton Fine-Structure Splittings in Single Perovskite Nanocrystals. *Physical Review Letters* **2017**, *119* (2). https://doi.org/10.1103/PhysRevLett.119.026401.

(32) Becker, M. A.; Vaxenburg, R.; Nedelcu, G.; Sercel, P. C.; Shabaev, A.; Mehl, M. J.; Michopoulos, J. G.; Lambrakos, S. G.; Bernstein, N.; Lyons, J. L.; et al. Bright Triplet Excitons in Caesium Lead Halide Perovskites. *Nature* **2018**, *553* (7687), 189–193. https://doi.org/10.1038/nature25147.

(33) Ramade, J.; Andriambariarijaona, L. M.; Steinmetz, V.; Goubet, N.; Legrand, L.; Barisien, T.; Bernardot, F.; Testelin, C.; Lhuillier, E.; Bramati, A.; et al. Fine Structure of Excitons and Electron–Hole Exchange Energy in Polymorphic $CsPbBr_3$ Single Nanocrystals. *Nanoscale* **2018**, *10* (14), 6393–6401. https://doi.org/10.1039/C7NR09334A.

(34) Butkus, J.; Vashishtha, P.; Chen, K.; Gallaher, J. K.; Prasad, S. K. K.; Metin, D. Z.; Laufersky, G.; Gaston, N.; Halpert, J. E.; Hodgkiss, J. M. The Evolution of Quantum Confinement in $CsPbBr_3$ Perovskite Nanocrystals. *Chem. Mater.* **2017**, *29* (8), 3644–3652. https://doi.org/10.1021/acs.chemmater.7b00478.

(35) Feng, F.; Nguyen, L. T.; Nasilowski, M.; Nadal, B.; Dubertret, B.; Coolen, L.; Maître, A. Consequence of Shape Elongation on Emission Asymmetry for Colloidal CdSe/CdS Nanoplatelets. *Nano Res.* **2018**, *11* (7), 3593–3602. https://doi.org/10.1007/s12274-017-1926-3.

(36) Rossi, D.; Wang, H.; Dong, Y.; Qiao, T.; Qian, X.; Son, D. H. Light-Induced Activation of Forbidden Exciton Transition in Strongly Confined Perovskite Quantum Dots. *ACS Nano* **2018**, *12* (12), 12436–12443. https://doi.org/10.1021/acsnano.8b06649.

(37) Chen, J.; Zhang, Q.; Shi, J.; Zhang, S.; Du, W.; Mi, Y.; Shang, Q.; Liu, P.; Sui, X.; Wu, X.; et al. Room Temperature Continuous-Wave Excited Biexciton Emission in Perovskite Nanoplatelets via Plasmonic Nonlinear Fano Resonance. *Commun Phys* **2019**, *2* (1), 80. https://doi.org/10.1038/s42005-019-0178-9.

(38) Rainò, G.; Nedelcu, G.; Protesescu, L.; Bodnarchuk, M. I.; Kovalenko, M. V.; Mahrt, R. F.; Stöferle, T. Single Cesium Lead Halide Perovskite Nanocrystals at Low Temperature: Fast Single-Photon Emission, Reduced Blinking, and Exciton Fine Structure. *ACS Nano* **2016**, *10* (2), 2485–2490. https://doi.org/10.1021/acsnano.5b07328.

(39) Ben Aich, R.; Saïdi, I.; Ben Radhia, S.; Boujdaria, K.; Barisien, T.; Legrand, L.; Bernardot, F.; Chamarro, M.; Testelin, C. Bright-Exciton Splittings in Inorganic Cesium Lead Halide Perovskite Nanocrystals. *Phys. Rev. Applied* **2019**, *11* (3), 034042. https://doi.org/10.1103/PhysRevApplied.11.034042.
(40) Brennan, M. C.; Kuno, M.; Rouvimov, S. Crystal Structure of Individual CsPbBr3 Perovskite Nanocubes. *Inorg. Chem.* **2019**, *58* (2), 1555–1560. https://doi.org/10.1021/acs.inorgchem.8b03078.
(41) Nestoklon, M. O.; Goupalov, S. V.; Dzhioev, R. I.; Ken, O. S.; Korenev, V. L.; Kusrayev, Yu. G.; Sapega, V. F.; de Weerd, C.; Gomez, L.; Gregorkiewicz, T.; et al. Optical Orientation and Alignment of Excitons in Ensembles of Inorganic Perovskite Nanocrystals. *Physical Review B* **2018**, *97* (23). https://doi.org/10.1103/PhysRevB.97.235304.
(42) Fu, M.; Tamarat, P.; Huang, H.; Even, J.; Rogach, A. L.; Lounis, B. Neutral and Charged Exciton Fine Structure in Single Lead Halide Perovskite Nanocrystals Revealed by Magneto-Optical Spectroscopy. *Nano Lett.* **2017**, *17* (5), 2895–2901. https://doi.org/10.1021/acs.nanolett.7b00064.